Materials Advances

ROYAL SOCIETY OF CHEMISTRY

PAPER

View Article Online
View Journal | View Issue

Cite this: *Mater. Adv.*, 2023, 4, 2487

A new copper molybdate-doped aluminium phosphate nanocomposite heterostructure for photoreduction of aqueous 2-NA and 4-NA†

Tanmay Kumar Ghorai,* Saumadip Chakraborty, Nilesh Satpute, Sajid Mehmood, Niteesh Kumar, Sanjay Kumar Sahu and Mithun Kumar Ghosh

Metal molybdate-doped aluminium phosphate ($M_xMo_xAl_{1-x}P_{1-x}O_4$; M = Cu, Ni, and Co) heterostructures have been prepared by a solid solution method and found to be efficient catalysts for the photoreduction of *o*-nitroaniline (*o*-NA) and *p*-nitroaniline (*p*-NA). A comparative investigation of the different metal molybdate-doped aluminium phosphate materials shows the photocatalytic activity of various proportions of copper/nickel/cobalt–molybdenum–aluminium–phosphorous oxides in the reduction of *o*-nitroaniline (*o*-NA) and *p*-nitroaniline (*p*-NA) under both UV and visible light. Among the three types of metal systems, the copper heterostructure is very effective ($Cu_xMo_xAl_{1-x}P_{1-x}O_4$)($x$ = 0.5) (CuMAP2), showing good results with very effective catalytic activity, photoluminescence (highest intensity peak at 271 nm) and semiconductor (E_g 4.21 eV) properties. Therefore, our main investigation focused on the copper system. The nanocomposites were characterized using UV-vis spectroscopy, X-ray diffraction (XRD), FT-IR spectroscopy and PL spectroscopy. The average crystallite and particle sizes of CuMAP2 were found to be 21.23 ± 1 and 45 ± 5 nm, respectively. Among the studied compositions, CuMAP2 showed the highest catalytic activity in the reduction of *o*-NA or 2-NA and *p*-NA or 4-NA under visible light. XRD analysis clearly explained the phase formation temperature and showed that different metal ions are present in the composition, which was also supported by FTIR spectroscopy. Photocatalytic parameters, including dopant concentration, catalyst loading, and *p*-NA and *o*-NA concentrations, have also been investigated.

Received 1st April 2023,
Accepted 15th May 2023

DOI: 10.1039/d3ma00152k

rsc.li/materials-advances

1. Introduction

Copper molybdate ($CuMoO_4$) is an interesting compound because of its catalytic, structural, and electronic properties.[1,2] Transition metal molybdates ($AMoO_4$) (A = Ni, Co, Fe, and Cu) are promising catalysts for oxidative dehydrogenation: particularly in the case of propane to propene[3,4] and several types of photochemical reactions, *i.e.* the degradation of different organic dyes (*i.e.* MO, RhB, TB, BG *etc.*). Most of the molybdate compounds exhibit high catalytic activity for the conversion of CO to CO_2. It has been demonstrated that copper molybdate systems have significant potential for reducing the carbon black combustion temperature.[5,6] When the surface of molybdate particles combines with solid carbon to generate surface $CuMoO_{4-x}$ phases with a high oxygen vacancy concentration, Cu(II) is reduced to Cu(I), which is the basic catalytic function of $CuMoO_4$.[6] Investigating how different cations affect the catalytic characteristics is interesting. Such frequent variation of oxidation state in the Ni or Co system is not observed.

In many acid–base, polymerization, redox, photocatalytic and alkylation processes, metal phosphates have great catalytic applications.[7] However, except for aluminium phosphate, these compounds have not been employed as catalytic supports. Even the use of aluminium phosphate has received little attention.

Metal-doped mixed oxides play an important role in many modern technologies. Commercial processes such as cracking, hydrogenation, dehydrogenation, oxidative dehydrogenation, and regeneration use these catalysts.[8] $M_xAl_{1-x}MoO_4$ (M = transition metal) is mainly employed in catalytic applications and has exceptional electrical and magnetic properties.[9,10] Previously, Ghorai *et al.* investigated the phase formation temperature and photocatalytic activity of $M_xCr_{1-x}Mo_xP_{1-x}O_4$ (M = Co, Ni and Cu) toward *p*-nitrophenol[11] and thymol blue.[12] Now, we are very much interested in the new composition of $M_xMo_xAl_{1-x}P_{1-x}O_4$ (M = Cu, Ni, and Co) and studying its photocatalytic activity, which has as yet not been studied in the literature.

In addition to being poisonous, 4-nitroaniline is dangerous due to its chemical stability. The treatment and disposal of waste

Nanomaterials and Crystal Design Laboratory, Department of Chemistry, Indira Gandhi National Tribal University, Amarkantak, Madhya Pradesh 484887, India. E-mail: tanmay.ghorai@igntu.ac.in, tanmayghorai66@gmail.com; Fax: 07629-269712; Tel: +919432512461

† Electronic supplementary information (ESI) available. See DOI: https://doi.org/10.1039/d3ma00152k

water that contains 4-nitroaniline has become a significant environmental issue.[13] Moreover, it demonstrates mutagenicity, carcinogenicity and toxicity towards several experimental model species.[14] As a result, several industrialised and developing nations have designated 4-nitroaniline as a priority pollutant and placed limitations on its manufacture, use, and disposal.[15] 4-Nitroaniline metabolites are non-biodegradable or slowly biodegradable and have varying toxicities toward aquatic life and higher organisms.[16–18] Several industrial compounds contain aminobenzenes as key constituents. *P*-Phenylenediamine (PPD), a compound that belongs to the class of aminobenzenes, is mostly employed as a component of rubber antioxidants and colours.[19] It serves as a precursor to thermoplastics and aromatic textile fibers. In a commercial procedure, 4-nitroaniline (4-NA) is nearly invariably used in the first step in the manufacture of *p*-Phenylenediamine (PPD), which is then catalytically hydrogenated.[20] These approaches are, however, constrained by strict reaction conditions, high costs, and time-consuming processes. *o*-Phenylenediamine (OPD) is a chemical intermediate used in the synthesis of fungicides, corrosion inhibitors, pigments and pharmaceuticals. OPD is also used to remove elemental sulfur in mining ores, and to remove aldehyde colour formers in polymeric products and colorimetric H_2O_2 detection.[21] OPD condenses with ketones and aldehydes to give rise to a variety of useful products. Photocatalysis has drawn a lot of attention in the realm of organic synthesis since it fits practically all of the proposed criteria for green chemistry. Water is the "greenest" solvent among all the solvents, and hence it is practicable to prepare PPD and OPD using photocatalysis in water.[22–26]

In this context, we report the synthesis and characterization of $Cu_xMo_xAl_{1-x}P_{1-x}O_4$ (where x = 0.1, 0.5 and 0.9) nanocomposites prepared by a solid solution method. The $Cu_xMo_xAl_{1-x}P_{1-x}O_4$ (x = 0.5) (CAMP2) solid solution showed excellent photocatalytic activity toward 2-NA and 4-NA in solution in the presence of both UV/visible light compared with the other compositions of $Cu_xMo_xAl_{1-x}P_{1-x}O_4$ (x = 0.1) (CAMP1), $Cu_xMo_xAl_{1-x}P_{1-x}O_4$ (x = 0.9) (CAMP3), $CuMoO_4$ (CM) and $AlPO_4$ (AP). XRD, UV-visible spectroscopy and FT-IR spectroscopy were used to evaluate the nanoscale photocatalysts.

2. Experimental section

2.1. Chemicals required

Ammonium molybdate $[(NH_4)_6Mo_7O_{24}\cdot4H_2O]$ (analytical reagent), copper nitrate trihydrate $[Cu(NO_3)_2\cdot3H_2O]$ (analytical reagent), $[Ni(NO_3)_2\cdot6H_2O]$ (analytical reagent), $[Co(NO_3)_2\cdot6H_2O]$ (analytical reagent), $Al(NO_3)_3\cdot9H_2O$ (analytical reagent), NaH_2PO_4 (analytical reagent), distilled water, NH_4OH (25%), HNO_3 (40%), triethanolamine (TEA), 4-nitroaniline (4-NA) and 2-nitroaniline (2-NA) were essential analytical reagents for this experiment.

2.2. Synthesis of $Cu_xMo_xAl_{1-x}P_{1-x}O_4$ nanocomposites

Nanoclusters of $Cu_xMo_xAl_{1-x}P_{1-x}O_4$ (x = 0.1, 0.5, and 0.9) were synthesized by a solid solution process. Two steps were taken to complete the whole synthesis. $CuMoO_4$, $Al(NO_3)_3\cdot9H_2O$, and NaH_2PO_4 stock solutions were made in the first phase. The procedure listed below was used to create the $CuMoO_4$ solution. Ammonium molybdate (1.235 g, mmol) was dissolved in 40% HNO_3 and distilled water in a 250 ml beaker. $[Cu(NO_3)_2\cdot3H_2O]$ (1.692 g, mmol) was dissolved in distilled water. Then, this solution was mixed with the first solution. After that, a 25% NH_4OH solution was used to precipitate the transparent copper solution while keeping the solution's pH in the 8–9 range. The precipitate was carefully filtered, rinsed in distilled water, and dried.

In the second step, stoichiometric amounts of copper molybdate, aluminium nitrate, and sodium dihydrogen phosphate with triethanolamine (6 ml) solutions and distilled water (10 ml) were taken in a beaker as per the predetermined chemical compositions and subjected to constant stirring for 20 min at room temperature. The mixed solution was dried at 200 °C to produce a black carbonaceous light porous mass, which was then calcined for two hours at three different temperatures, 500 °C, 600 °C, and 700 °C, at a heating rate of 5 °C min^{-1}, for different chemical compositions of $Cu_xMo_xAl_{1-x}P_{1-x}O_4$ (x = 0.1, 0.5, and 0.9) nano-powders. By following the same procedure, we synthesized the $Co_xMo_xAl_{1-x}P_{1-x}O_4$ and $Ni_xMo_xAl_{1-x}P_{1-x}O_4$ (x = 0.5) nanocomposites. Flowchart S1 (ESI†) shows the entire synthesis process.

2.3. Photocatalytic activity

The photocatalytic activities of the newly prepared nanosized $Cu_xMo_xAl_{1-x}P_{1-x}O_4$ (x = 0.1, 0.5 and 0.9) powders were characterized using the photodegradation of 2-nitroaniline and 4-nitroaniline to OPD and PPD, respectively, in aerated aqueous solution as a model photoreaction. The photocatalytic reactions were carried out with simultaneous irradiation by UV-visible light in an advanced microprocessor (UV-vis spectrophotometer single beam LI-295). The reactions were performed by adding nanopowders of each photocatalyst (0.0015 g) into each set of 10 mL samples of 2-nitroaniline and 4-nitroaniline. The time of reduction in both cases for different compositions is given below. All the combinations of catalyst and 2-nitroaniline and 4-nitroaniline were subjected to UV-vis irradiation for 8 min in 2 min intervals.

2.4. Characterization of the nanocatalysts

By employing an X-ray diffractometer (XRD) at room temperature with Cu K as the target material, 40 kV accelerating voltage, 30 mA emission current, and a 40 min scanning speed, the crystal structure of the produced photocatalysts was determined. A Si crystal's XRD pattern was utilized as a reference to calibrate the scanning angles. The fine structure of the prepared powders was analyzed using FT-IR spectroscopy. Absorbance of 2-nitroaniline and 4-nitroaniline was measured with the help of a UV–Vis spectrophotometer single beam LI-295.

3. Results and discussion

3.1. XRD analysis

The crystalline phase and particle size of the novel metal molybdate $MMoO_4$ (M = Cu, Co, and Ni)-doped aluminium phosphate

nanocomposite were investigated using XRD (X-ray diffraction). The XRD patterns of $Cu_xMo_xAl_{1-x}P_{1-x}O_4$ (CuMAP2), $Ni_xMo_xAl_{1-x}P_{1-x}O_4$ (NiMAP), and $Co_xMo_xAl_{1-x}P_{1-x}O_4$ (CoMAP) (x = 0.5) (Cu-Kα radiation, λ = 1.54060 Å) are shown in Fig. 1. As shown in Fig. 1(a), the peaks at 2θ values of 14.097°, 19.587°, 26.321°, 29.418° and 34.643° can be assigned to (110), (210), (210), (031), (111) and (221), respectively, for CuMAP2 according to JCPDF Card No. 360405. The peaks at 2θ values of 14.08°, 19.66°, 26.25°, 28.53°, 29.43° and 34.75° were assigned to (110), (210), (101), (121), (003) and (−103), respectively, for CoMAP according to JCPDF Card No. 130128, as shown in Fig. 1(b). The peaks at 2θ values of 14.41°, 25.31°, 28.99°, 32.87°, 37.33°, 43.71°, and 47.45° were assigned to (110), (121), (220), (222), (200), (330) and (204), respectively, for NiMAP, as shown in Fig. 1(c), according to JCPDF Card No. 210868. In all three cases, the X-ray patterns of the synthesized composites match well with JCPDF No. 500054, indicating the formation of $AlPO_4$ in the composites. For all cases, similar 2θ values arise at 20.51°, 21.99°, 23.78°, 30.43° and 35.33° that can be assigned to (210), (211), (121), (104) and (321), respectively. Therefore $CuMoO_4$/$CoMoO_4$/$NiMoO_4$-doped $AlPO_4$ should be good materials for catalytic applications. The remarkable observation was found that, - $Cu_xMo_xAl_{1-x}P_{1-x}O_4$ as well as the other metal composites, the catalytic performance is maximum at x = 0.5 and therefore we mainly focused our study on the CuMAP2 composite. The crystalline sizes of the CuMAP2, CoMAP and NiMAP nanocomposites were calculated from the Scherrer formula and were found to be 21.23, 22.45, and 19.73 nm using the (111), (003) and (220) peaks, respectively. The XRD pattern of the mother compound of $CuMoO_4$ is presented in Fig. S1 (ESI†) for comparison purposes of the different metal-doped $AlPO_4$ nanocomposites (shown in Fig. S2, ESI†).

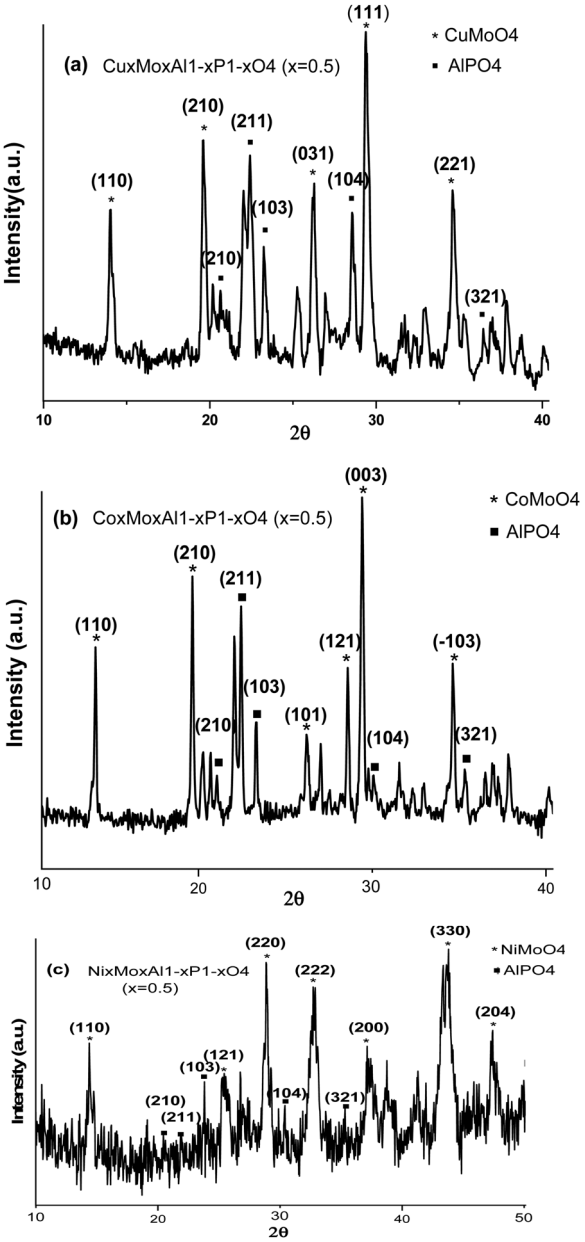

Fig. 1 XRD patterns of (a) CuMAP2, (b) CoMAP, and (c) NiMAP at 700 °C.

3.2. FT-IR spectral analysis

The FT-IR spectra of the CuMAP1, CuMAP2, CuMAP3 and $CuMoO_4$ samples are depicted in Fig. 2. The two bands observed at about 3430–3450 cm^{-1} and 1630–1636 cm^{-1} are characteristic of the H–O bending mode of hydroxyl groups present on the surface due to moisture. The asymmetric stretching vibration of the Mo═O···Mo bridge appears at around 801–832 cm^{-1}. The peaks that appear at 1120–1130 cm^{-1} are due to the antisymmetric stretching vibration of Al–PO_4 groups. The strong band at 500–532 cm^{-1} probably arises from stretching modes of Cu–O bands. These data indirectly indicate that $CuMoO_4$ has been dissolved into the $AlPO_4$ lattice. Among all the composites, we have only described $Cu_xMo_xAl_{1-x}P_{1-x}O_4$ (x = 0.5) (CuMAP2) in the manuscript and not the other composites of $CuMoO_4$-doped $AlPO_4$ and Co and Ni molybdate-doped $AlPO_4$ because of their lower catalytic activity.

3.3. TEM analysis of $Cu_xMo_xAl_{1-x}P_{1-x}O_4$ (x = 0.5) (CuMAP2)

Fig. 3 shows the TEM images of various composites of metal molybdate-doped aluminium phosphate nanocomposites. Fig. 3(a) shows the spherical nanoparticles of CuMAP1. Fig. 3b–d show the different images of CuMAP2 with a spherical

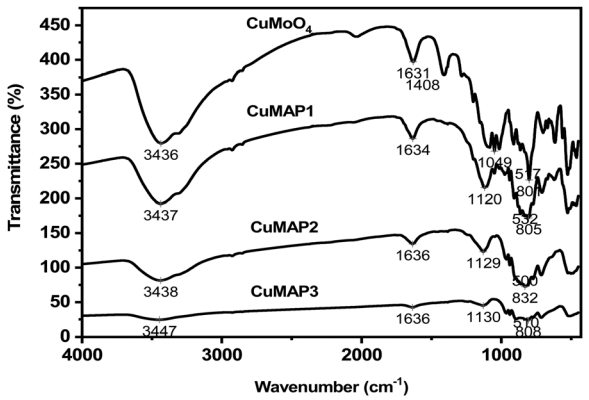

Fig. 2 FT-IR spectra of CuMAP1, CuMAP2, CuMAP3 and $CuMoO_4$.

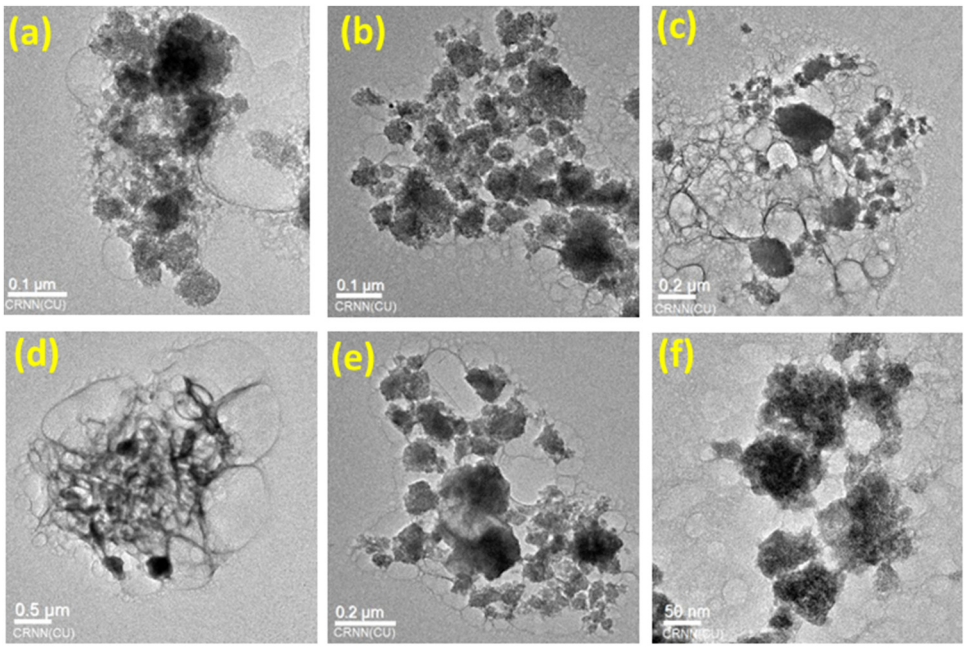

Fig. 3 TEM images of (a) CuMAP1, (b–d) CuMAP2, (e) CoMAP, and (f) NiMAP.

shape as well as thin hair type spiral nanoparticles. Interestingly, Fig. 3(d) shows a beautiful spiral bunch of hair and the inset indicates the spherical nature of CuMAP2. Fig. 3(e) and (f) depict the particle shape of the CoMAP and NiMAP nanocomposites, respectively. The TEM images show the beautiful shape of the nanoparticles of CuMAP2, which shows better photocatalytic activity compared to the other catalysts, and that its average particle size is 45 ± 5 nm (Fig. 3b).

3.4. Optical properties

Fig. 4(a) depicts the band structure of the nanocatalysts obtained from UV-vis spectroscopy measurement, which was used to characterize the absorption edge and band gap energy. Here, we applied Tauc's formula presented in eqn (1) to calculate the band gap energy of these nanocatalysts.

$$(\alpha h\upsilon)^n = A(h\upsilon - E_g) \quad (1)$$

where A is a constant, α signifies the absorption coefficient, Plank's constant is indicated by h, the band gap energy is indicated by E_g, and exponent n is dependent on the type of transition.

The calculated optical energy band gap of $Cu_xMo_xAl_{1-x}P_{1-x}O_4$ (x = 0.5) is 4.21 eV [Fig. 4(a)]. The other band gap values of the nanocatalysts were 5.00, 4.61, 4.30 and 4.50 eV for $Cu_xMo_xAl_{1-x}P_{1-x}O_4$ (x = 0.1), $Cu_xMo_xAl_{1-x}P_{1-x}O_4$ (x = 0.9), $Co_xMo_xAl_{1-x}P_{1-x}O_4$ (x = 0.5) and $Ni_xMo_xAl_{1-x}P_{1-x}O_4$ (x = 0.5), respectively. The optical band gap values reveal that the nanocatalysts are semiconducting in nature. Among all the catalysts, $Cu_xMo_xAl_{1-x}P_{1-x}O_4$ (x = 0.5) shows the lowest band gap value and highest photodegradation performance because of faster electron transfer from valence band to conduction band.

To analyse the various kinds of defects present, room temperature photoluminescence (PL) spectra of CuMAP2, NiMAP and CoMAP were recorded at an excitation wavelength of 287 nm (Fig. 4b). The maximum intensity peak of the nanocatalysts appeared at 571 nm. From the PL spectra, it is clear that at the highest intensity peak of 571 nm, the nanocatalysts have better photoluminescence properties. Better photoluminescence properties were observed in the CoMAP system compared to the others.

3.5. Photocatalytic activity of $Cu_xMo_xAl_{1-x}P_{1-x}O_4$ (CuMAP)

Each of the five sets of 50 mL beakers holding 10 mL of aqueous solutions of 2-nitroaniline (2-NA) and 4-nitroaniline (4-NA) had a freshly made aqueous solution of NaBH4 (0.502 mol dm^{-3}) added to it. In aqueous medium, 2-NA and 4-NA dissolved slowly forming a light-yellow solution. Upon addition of $NaBH_4$, dissolution was quick with the development of a deep yellow colour. In the absence of catalysts, 2-NA and 4-NA were reduced to OPD and PPD very slowly under UV light. In the absence of $NaBH_4$, $Cu_xMo_xAl_{1-x}P_{1-x}O_4$ (CuMAP2) showed no catalytic activity. Then, 0.0015 g of each of the $Cu_xMo_xAl_{1-x}P_{1-x}O_4$ nanocatalysts was added to 10 ml of both solutions and the catalytic reduction was examined. Fig. 5(a) and (b) represent the reduction of 2-NA and 4-NA in the presence of CuMAP2, NiMAP and CoMAP, and it was found that in both cases CuMAP2 shows good reduction efficiency compared to the NiMAP and COMAP catalysts. Fig. 5(c) illustrates the catalyst loading optimization in the presence of 2-NA/4-NA and it was found that when catalyst loading was 0.0015 g/10 mL, the catalytic efficiency was maximum and lower and higher loading amounts of catalyst did not show significant results. Fig. 6(a) and (c) show the kinetics of the reaction or reaction rate constant at constant intervals and Fig. 6(b) and (d) show the corresponding UV-visible spectra we used to measure the concentration of 2-NA and 4-NA. The inset of Fig. 5b and d shows the reduction of 2-NA

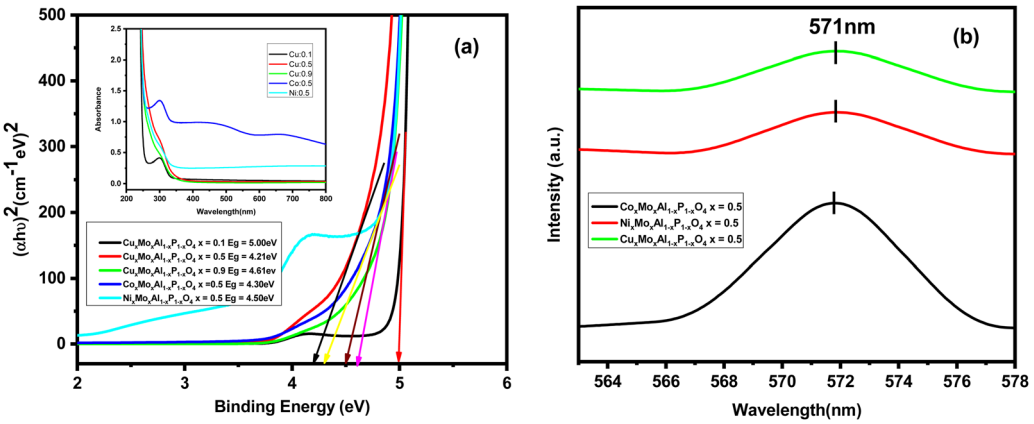

Fig. 4 (a) Band gap and (b) PL spectra of the nanocatalysts.

and 4-NA at small time intervals (2 min) in the presence of $Cu_xAl_{1-x}Mo_xP_{1-x}O_4$ ($x = 0.5$) (CuMAP2). As a consequence, it can be seen that in both cases, the yellow colour of 2-NA and 4-NA vanished under the influence of CuMAP2 and UV light within 8 minutes. The other compositions of CuMAP1 and CuMAP3 took much more time, *i.e.* 35 and 15 min (ESI† Fig. S3–S6), for the formation of OPD and PPD in the presence of UV light, compared to the mother compounds $CuMoO_4$ and $AlPO_4$ (ESI† Fig. S7–S10). In the UV-vis spectra of 2-NA, the CuMAP2 catalyst significantly reduced the peak at 412 nm and increased the peak at 282 nm (Fig. 6b). In the UV-vis spectra of 4-NA, the CuMAP2 catalyst significantly reduced the absorption peak at 378 nm and increased the absorbance peak at 224 nm (Fig. 6d). Both times, as the light shifted to its peak location, the yellow colour disappeared during the reduction period at the same time that OPD and PPD simultaneously formed. A new peak appearing at 308 nm was assigned to the conversion of 4-NP to PPD (*p*-phenylenediamine) in the UV-vis spectra but no such new peak arose on conversion of 2-NP to OPD. The conversion values of 4-NP to PPD and 2-NP to OPD by CuMAP2 are 92% and 79%, respectively.

When using 2-NA, the kinetics of this reaction can be quantitatively monitored by observing the progression of the

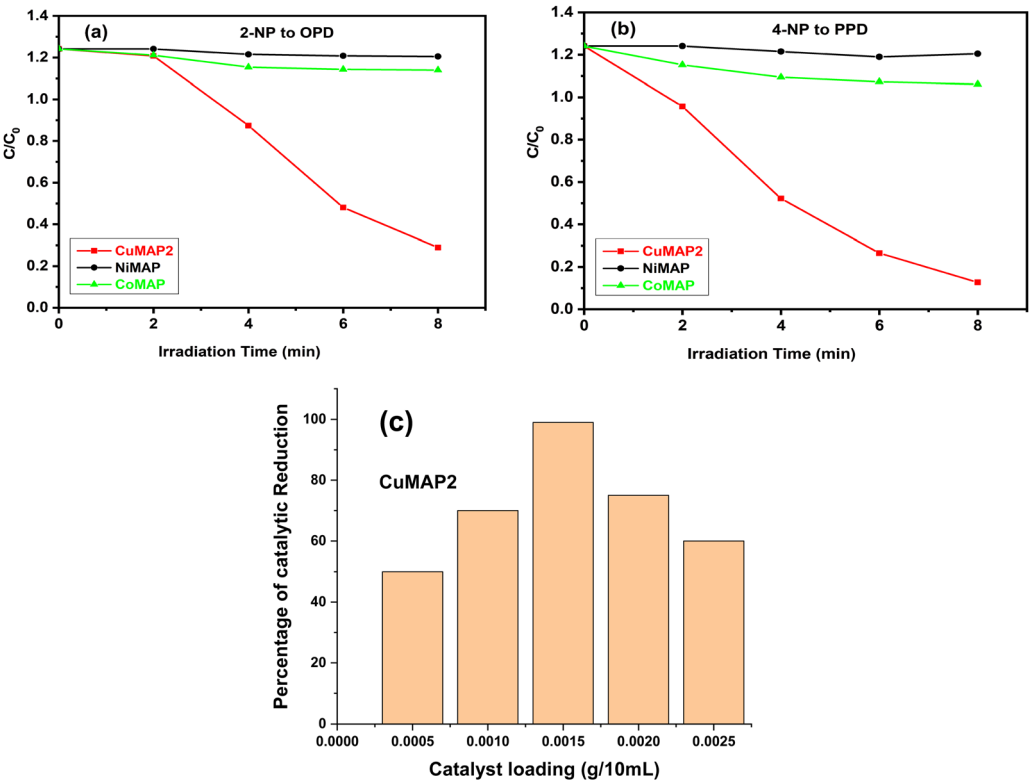

Fig. 5 (a) Reduction of 2-NA in the presence of CuMAP2, NiMAP and CoMAP, (b) reduction of 4-NA in the presence of CuMAP2, NiMAP and CoMAP, and (c) catalyst loading optimization in the presence of 2-NA/4-NA.

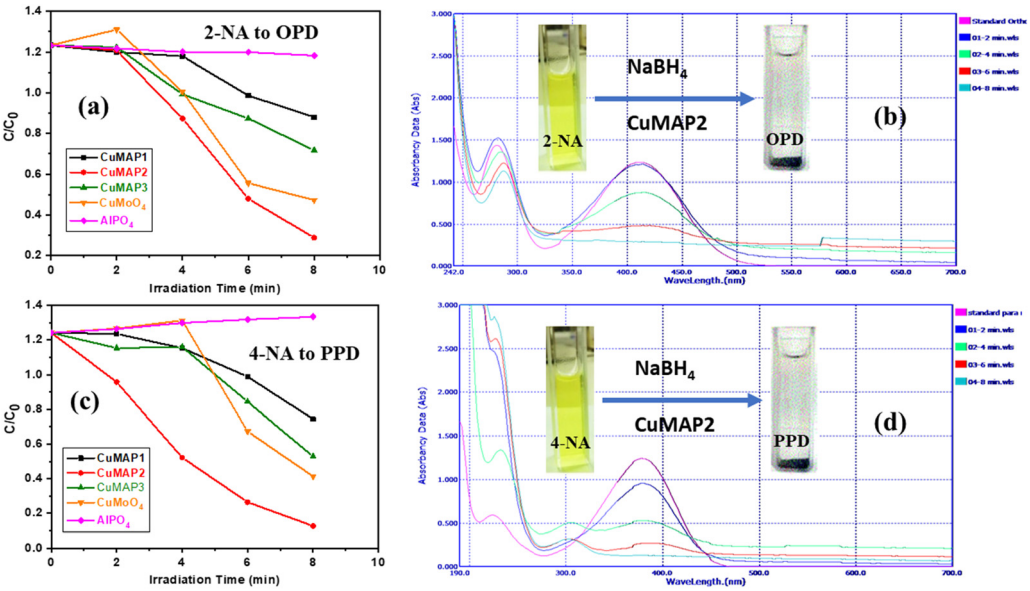

Fig. 6 (a) Reaction rate constant of 2-NA reduction in the presence of CuMAP1, CuMAP2, CuMAP3, $CuMoO_4$, and $AlPO_4$ under UV and visible light, (b) change in concentration of 2-NA and corresponding UV absorption spectra in the presence of CuMAP2, (c) reaction rate constant of 4-NA reduction in the presence of CuMAP1, CuMAP2, CuMAP3, $CuMoO_4$, and $AlPO_4$ under UV and visible light and (d) change in concentration of 4-NA and corresponding UV absorption spectra in the presence of CuMAP2.

peak intensity at 412 nm with time. The following equation can be used to obtain the reaction's kinetics:

$$ln\frac{[C]}{[C_O]} = -kt \quad (2)$$

where k = rate constant, t = reaction time, $[C_o]$ = concentration of 2-NA at time t = 0 and $[C]$ = concentration at time t. The absorbance of the peaks at 412 and 378 nm can be used to determine the value of $[C]$. Plots of absorbance *vs.* time (min) for the catalytic reduction of 2-NA and 4-NA under different reaction conditions are shown in Fig. 6a and b. The slope of the plot of $\ln(C/C_0)$ as a function of time was used to calculate the value of k for the reduction of 2-NA and 4-NA. The rate constants of CAMP1, CAMP2, CAMP3, CoMAP, NiMAP, CuM and AP were measured after 50% degradation and complete reduction of 2-NA and 4-NA to OPD and PPD, and are shown in Table 1, respectively. Therefore, in both cases, CuMAP2 gives much faster reaction kinetics (87.648×10^{-3} min^{-1} for 2-NA and 216.510×10^{-3} min^{-1} for 4-NA) than that of CuMAP1, CuMAP3, $CuMoO_4$ (CuM) and $AlPO_4$ (AP).

After completion of the first run, CuMAP2 nanocatalyst was recovered by simple filtration. The recovered catalyst was washed repeatedly with DDW and ethanol and dried at 100 °C in a hot air oven for reuse. The recyclability of the nanocatalyst was studied for conversion of 4-NP to PPD under the same reaction conditions. The nanocatalyst was recovered and reused in two more subsequent runs without appreciable loss of photocatalytic activity (ESI† Fig. S11).

3.6. Proposed mechanism

This process can be catalytically improved by metals. It is widely known that $NaBH_4$ works as a hydrogen source that releases hydrogen gas by hydrolysis at normal temperature. It is well known that metal nanoparticles, such as those made of copper, platinum, silver, and gold, accelerate the transfer of electrons from donors (in this case, BH_4^-) to acceptors (2-NA/4-NA). The 2/4-nitrophenolate ions and BH_4^- ions must first bind to the catalyst surface in order for this reduction process to occur. The reduction process is made relatively simple by the near proximity of the reactive groups on the catalyst surface.[11,12] Here, the $Cu_xMo_xAl_{1-x}P_{1-x}O_4$ catalyst provided the adsorption sites for

Table 1 The crystallite size, reaction rate constant and degradation time of CAMP1, CAMP2, CAMP3, CoMAP, NiMAP, CuM and AP are presented

Compounds	Abbreviation	Reaction composition	Crystallite size (nm)	Reaction rate constant k ($\times 10^{-3}$ min^{-1})		Time required for degradation (min)	
				2-NA	4-NA	2-NA	4-NA
$Cu_xMo_x Al_{1-x}P_{1-x}O_4$ (x = 0.1)	CuMAP1	CuMAP2 + $NaBH_4$ + 2-NA/4-NA	21.23 ± 1	12.812	18.387	35	30
$Cu_xMo_x Al_{1-x}P_{1-x}O_4$ (x = 0.5)	CuMAP2	CuMAP2 + $NaBH_4$ + 2-NA/4-NA	21.23 ± 1	87.648	216.501	8	8
$Cu_xMo_x Al_{1-x}P_{1-x}O_4$ (x = 0.9)	CuMAP3	CuMAP2 + $NaBH_4$ + 2-NA/4-NA	20.99 ± 1	55.735	17.089	15	15
$Co_xMo_x Al_{1-x}P_{1-x}O_4$ (x = 0.5)	CoMAP	CuMAP2 + $NaBH_4$ + 2-NA/4-NA	22.45 ± 1	18.170	31.519	—	—
$Ni_xMo_x Al_{1-x}P_{1-x}O_4$ (x = 0.5)	NiMAP	NiMAP2 + $NaBH_4$ + 2-NA/4-NA	19.73 ± 1	4.677	5.293	—	—
$CuMoO_4$	CuM	CuM + $NaBH_4$ + 2-NA/4-NA	20.11 ± 1	52.735	22.082	12	10
$AlPO_4$	AP	AP + $NaBH_4$ + 2-NA/4-NA	18.22 ± 1	8.399	−11.226	—	—

BH_4^- ions as well as for the nitro aromatic compounds and also assisted in the transfer of electrons from the donor BH_4^- ions to the nitro aromatic compound (acceptor). In the present case, electron transfer takes place from BH_4^- to 2/4-NA through adsorption of the reactant molecules on to the catalyst surface. H–Cu and $CuBH_3^-$ have been proposed as reactive intermediates in the catalytic breakdown of BH_4^- by $Cu_xMo_xAl_{1-x}P_{1-x}O4$ eqn (3).

$$2Cu + BH_4^- \leftrightarrow Cu - BH_3^- + Cu - H \quad (3)$$

The conversion of *p*-NA to PPD is thought to be caused by these species (eqn (4) and (5) to convert *p*-NA to PPD stoichiometrically, a six-electron reduction is needed).

$$6H - Cu + p - NA \rightarrow p - PD + 6Cu + 6H^+ \quad (4)$$

$$6Cu - BH_3^- + p - NA \rightarrow p - PD + 6Cu + 6BH_3 \quad (5)$$

Thus, when 4-NA/2-NA and BH_4^- ions were adsorbed on the surface of the nanocatalyst, the reduction occurred *via* relaying of electrons from the donor BH_4^- to the acceptor 4-NA/2-NA.[11,12]

4. Conclusion

In summary, we have developed a new copper molybdate ($CuMoO_4$)-doped aluminium phosphate ($Cu_xMo_xAl_{1-x}P_{1-x}O_4$) ($x$ = 0.1, 0.5, 0.9) nanocomposite by a co-precipitation method and initially found that the efficient photocatalytic reduction of 2-nitroaniline and 4-nitroaniline under UV light can be achieved. We have also prepared other metal composites like $Co_xMo_xAl_{1-x}P_{1-x}O_4$ and $Ni_xMo_xAl_{1-x}P_{1-x}O_4$ where x-0.5. Among all the composites, $Cu_xMo_xAl_{1-x}P_{1-x}O_4$ (x = 0.5) shows good catalytic reduction of 2-NA and 4-NA to OPD and PPD in the presence of UV light. The average crystallite and particle sizes of CuMAP2 were found to be 21.23 ± 1 and 45 ± 5 nm, respectively. This is a unique composite and it may have good electronic properties and it will be the subject of further study.

Author contributions

All the experiments and application were performed by S. Chakraborty, N. Satpute, S. Mehmood, N. Kumar, S. K. Sahu and M. K. Ghosh under the supervision of Dr T. K. Ghorai. The manuscript was written and corrected by Dr T.K. Ghorai.

Conflicts of interest

The authors declare no conflict of financial interest.

Acknowledgements

This work was fully supported by Madhya Pradesh Council of Science & Technology, Govt. of India, Madhya Pradesh (File No. A/R&D/RP-2/Phy & Engg./2017-18/271) and DST-FIST, Govt. of India, (File No. SR/FST/CS-I/2017/2(C)) is gratefully acknowledged for financial assistance to develop the Instrumental facility at Department of Chemistry, IGNTU. The authors are also thankful to University of Calcutta, WB and Indira Gandhi National Tribal University India for analysis of TEM, XRD and UV-Vis spectroscopy measurement.

References

1 L. Kamarasu, E. Sathiyamoorthi, S. S. Nannapaneni, S. Arunachalam, M. Arunpandian, J. Lee, P. Arumugam and N. K. Katari, *Phys. B*, 2023, **650**, 414544.
2 W. Tan and J. Luan, *RSC. Adv.*, 2020, **10**, 9745.
3 S. K. Ray and J. Hur, *J. Environ. Manage.*, 2021, **278**, 111562.
4 J. H. Carter, T. Bere, J. R. Pitchers, D. G. Hewes, B. D. Vandegehuchte, C. J. Kiely, S. H. Taylor and G. J. Hutchings, *Green Chem.*, 2021, **23**, 9747–9799.
5 Q. Qian, Y. Li, Y. Liu, Y. Guo, Z. Li, Y. Zhu and G. Zhang, *J. Chem. Eng.*, 2021, **414**, 128818.
6 A. Corma, *Chem. Rev.*, 1997, **97**, 2373.
7 U. Ciesla and F. Schüth, *Microporous Mesoporous Mater.*, 1997, **27**, 131–149.
8 B. S. Girgis, A. M. Youssef and M. N. Alaya, *Surf. Technol.*, 1980, **10**, 105–113.
9 S. K. Matam, C. Moffat, P. Hellier, M. Bowker, I. P. Silverwood, C. R. A. Catlow, D. Jackson, J. Craswell, P. P. Wells, S. F. Parker and E. K. Gibson, *Catalysts*, 2020, **10**, 1370.
10 J. Li, F. Li, J. Liao, Q. Liu and H. Li, *Catalysts*, 2019, **9**(9), 714.
11 T. K. Ghorai, *J. Mater. Res. Technol.*, 2015, **4**, 133–143.
12 T. K. Ghorai, D. Dhak, S. Dalai and P. Pramanik, *Appl. Catal.*, 2008, **339**, 137–144.
13 R. S. Nair, C. S. Auletta, R. E. Schroeder and F. R. Johannsen, *Fundam. Appl. Toxicol.*, 1990, **15**, 607–621.
14 G. Wang, X. Zhang, C. Yao and M. Tian, *Drug Chem. Toxicol.*, 2010, **33**, 238–243.
15 J. H. Sun, S. P. Sun, M. H. Fan, H. Q. Guo, L. P. Qiao and R. X. Sun, *J. Hazard. Mater.*, 2007, **148**, 172–177.
16 M. I. Din, R. Khalid, Z. Hussain, J. Najeeb, A. Sahrif, A. Intisar and E. Ahmed, *RSC Adv.*, 2020, **10**, 19041–19058.
17 L. G. Devi, N. Kottam and S. G. Kumar, *J. Phys. Chem. C*, 2009, **113**, 15593–15601.
18 J. Panpranot, K. Kontapakdee and P. Praserthdam, *J. Phys. Chem. B*, 2006, **110**, 8019–8024.
19 A. Sinha, S. K. Sahu, S. Biswas, M. Mandal, V. Mandal and T. K. Ghorai, *ACS Omega*, 2021, **6**(44), 29629–29640.
20 S. Naghash-Hamed, N. Arsalani and S. B. Mousavi, *ChemistryOpen*, 2022, **11**, 1–10.
21 Y. Liu, R. P. Lopes, T. Lüdtke, D. D. Silvio, S. Moya, J. R. Hamon and D. Astruc, *Inorg. Chem. Front.*, 2021, **8**, 3301–3307.
22 W. Wu, S. Liang, Y. Chen, L. Shen, H. Zheng and L. Wu, *Catal. Commun.*, 2012, **39**, 42.
23 M. Y. Qi, Z. R. Tang and Y. J. Xu, *ACS Catal.*, 2023, **13**, 3971–3982.
24 J. Y. Li, Y. H. Li, M. Y. Qi, Q. Lin, Z. R. Tang and Y. J. Xu, *ACS Catal.*, 2020, **10**, 6262–6280.
25 M. Y. Qi, M. Conte, M. Anpo, Z. R. Tang and Y. J. Xu, *Chem. Rev.*, 2021, **121**, 13051–13085.
26 M. Q. Yang and Y. J. Xu, *Phys. Chem. Chem. Phys.*, 2013, **15**, 19102–19118.